INTERNATIONAL JOURNAL OF ENERGY STUDIES

e-ISSN: 2717-7513 (ONLINE); homepage: https://dergipark.org.tr/en/pub/ijes

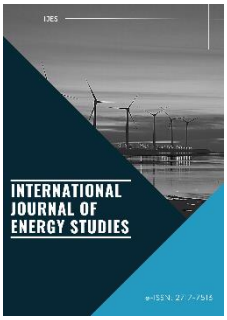

Research Article
Int J Energy Studies 2023; 8(2): 167-187
DOI: 10.58559/ijes.1263940

Received : 12 Mar 2023
Revised : 25 May 2023
Accepted : 26 May 2023

Heat transfer enhancement of a slot-confined and submerged impinging jet utilizing lamina-shaped $CoFe_3O_2$/water nanofluid

Recep Ekiciler*
Department of Mechanical Engineering, Gazi University, Ankara, Türkiye, ORCID: 0000-0003-1367-9465
*(*Corresponding Author: recepekiciler@gazi.edu.tr)*

Highlights

- The numerical study of a confined impinging slot jet in a nanofluid and water is presented.
- Increasing nanoparticle volume fractions of $CoFe_3O_2$/water led to a higher Nusselt number.
- It is best to use $CoFe_3O_2$/water at a volume concentration of 4.0%, and a Reynolds number of 24000.

You can cite this article as: Ekiciler R. Heat transfer enhancemente of a slot-confined and submerged impinging jet utilizing lamina shaped $CoFe_3O_2$/water nanofluid**.** Int J Energy Studies 2023; 8(2): 167-187.

ABSTRACT

Designing a cooling system is crucial for the thermal management of many different types of energy applications, such as fuel cells, solar panels, electronic cooling, and many more. A higher local heat transfer coefficient is attained by impinging jets, making them a viable cooling option. This study investigates a two-dimensional numerical study into the turbulent convective heat transfer in a confined slot and submerged impinging jet by using water and a nanofluid for Reynolds numbers between 6000 and 24000. The nanofluid of lamina-shaped $CoFe_3O_2$/water has been studied, with the volume concentration of nanoparticles ranging from 2.0% to 4.0%. Using a finite volume technique based on the SIMPLE algorithm, the governing momentum, continuity, and energy equations are solved. A presentation and discussion of the influence of the nanoparticle's volume fraction and the Reynolds number on the flow and thermal properties are provided. Increasing the volume fraction of nanoparticles is shown to enhance the Nusselt number and the Darcy friction factor. Entropy generation increases with the increase of the Reynolds number for all working fluids.

Keywords: Lamina-shaped, Confined, Submerged, Impinging surface, Nanofluid

1. INTRODUCTION

As computer devices, MEMS, turbomachinery, solar panels, and space technology continue to shrink in size while rising in power, there has been an uptick in research into effective hot spot cooling methods. The removal of large thermal power densities may be accomplished by using impinging jet cooling [1]. Extensive computational and experimental studies have been undertaken on impinging jets, but a perfect solution has not yet been found; further study is needed. As a result of growing discontent, researchers in the field of jet impingement are looking for other methods to improve the technology. There have been updates made to the jet, the target plate, and the operating fluid (nanofluid, oil, and two-phase fluid). Each of these new methods has the possibility of improving the impingement jet's hydraulic and thermal efficiency, making it more competitive with other technologies. Because of its increased thermal conductivity, nanofluid technology has found new applications. For impinging jets and other uses, it has great potential both now and in the future.

To learn more about the heat transfer properties of a horizontal circular plate with the Al_2O_3-water nanofluid, Zeitoun et al. [2] conducted experimental research. Experiments were conducted with a range of nanoparticle concentrations (between 6.6% and 10%), circular disk diameters, jet nozzle diameters, and jet flow rates. Increasing the concentration of nanoparticles is shown to result in a higher Nusselt number (*Nu*). Nguyen et al. [3] performed an experimental study on heat transmission via a submerged and confined impinging jet using Al_2O_3-water nanofluids; this work was connected to a previous study on nanofluids regarding the application of impingement jets. A range of jet pressure loss lengths, heat transfer coefficients, and flow velocities were tested and compared. Jet impingement cooling of a partially curved heated wall was studied by Selimefendigil and Oztop [4], who looked into the heat transfer characteristics of nanofluids under these conditions. They investigated how the concentration of nanoparticles affected the *Nu* required for the best-curved surface. It was shown that at larger values of the Reynolds number (*Re*), the impact of the curved wall on heat transfer qualities is more noticeable when compared to a flat surface. Adjusting the *Re*, impact angle, and plate-to-nozzle distance allowed researchers to study the heat transfer efficiency. The findings demonstrated a correlation between the convective heat transfer coefficient and the ease with which nanoparticles may be suspended in pure water. For a given nanoparticle concentration and *Re*, the convective heat transfer coefficient diminished as the attack angle increased. Furthermore, a link between the nanoparticles' impact on heat transfer and the state of the impinging jet was postulated. For their research, Tie et al. [5] used a

Cu/water nanofluid to examine the heat transmission in jet arrays upon impact. There was a range of 0.17 to 0.64% by volume of Cu nanoparticles and 0.05 to 0.1 weight percent of the dispersant sodium dodecyl benzoic sulfate (SDBS). In other words, their experiments showed that a higher concentration of nanofluid resulted in a better heat transfer coefficient. According to the research by Khatak et al. [6], ZnO nanofluid increased heat flow by about 20.2% while lowering the test sample's surface temperature by about 15%[6]. This indicated that the use of nanofluids as a means of cooling electronic components can significantly improve their performance. Heat transport and entropy generation in limited slot-jet impingement with TiO_2-water nanofluid were numerically studied by Lafouraki et al. [7]. An increase in the nanoparticle volume fraction's (*napv*'s) was shown to result in a higher rate of overall entropy creation. Coolants containing suspended Al_2O_3 nanoparticles were investigated numerically by Gherasim et al. [8] for their potential to improve heat transmission inside a constrained impinging jet cooling system. Researchers discovered that nanofluids might be used to improve heat transmission, although the increased pumping power that would be required to do so could restrict the application's potential. To further understand the function of several key controlling factors in the impingement jet, Abdullah et al. [9] performed experimental research under turbulent flow conditions. H/D and S/D are two such variables, and their respective ranges are 1–11 and 1–3, respectively. The primary hypothesis advanced by the experiments was that a high *Re* would result in maximum heat transfer. Singh et al. [10] conducted an experimental study on the cooling of a heated steel surface using laminar nanofluid jets. A comparative analysis is conducted on the cooling rates of nanofluids containing TiO_2, Al_2O_3, and SiO_2, which are characterized by identical concentrations and velocities. The present study assesses the impact of TiO_2-based nanofluid concentration and jet velocity on the cooling rate. The utilization of nanofluid jets has been observed to result in improved heat transfer in comparison to conventional water-based fluids. A free impingement of nano-jet flow was simulated numerically by Rehman et al. [11] across a heated square surface with homogeneous heat flux. The Volume of Fluid (VOF) multiphase model was implemented with nanofluid characteristics for a three-dimensional scenario. They got near the surface of the heater and utilized a standard $k - \varepsilon$ model for turbulence with a fine mesh.

In this study, numerical solutions for a confined and submerged impinging jet are obtained by running the CFD package program. The form of the nanoparticle has a significant impact on its thermal conductivity in suspension. For various heat transfer applications, since lamina-shaped nanofluids have better heat transfer abilities than spherical-shaped nanofluids, lamina-shaped

nanoparticles are chosen [12,13]. Lamina-shaped $CoFe_3O_2$/water nanofluid impingement jets have not been taken into account in previous research. Variations in *napv* and *Re* are studied for their impacts. This research improves our understanding of the cooling system by examining the impact of a confined and submerged impinging jet on the heat transfer of the impinging surface.

2. MODEL DESCRIPTION AND MATHEMATICAL FORMULATION

2.1. Physical Model

The jet impinges on a heated wall in the channel, as shown in Figure 1. The jet inlet width (W) and height (H) of the two-dimensional channel are respectively equal to 0.0062 m and 0.0248 m. The length (L) of the channel is equal to 0.31 m. The impingement bottom surface is kept at a constant temperature of 343 K. The fluid under consideration is a combination of water and lamina-shaped $CoFe_3O_2$ nanoparticles, with various *napv*s of $CoFe_3O_2$ between 2% and 4%.

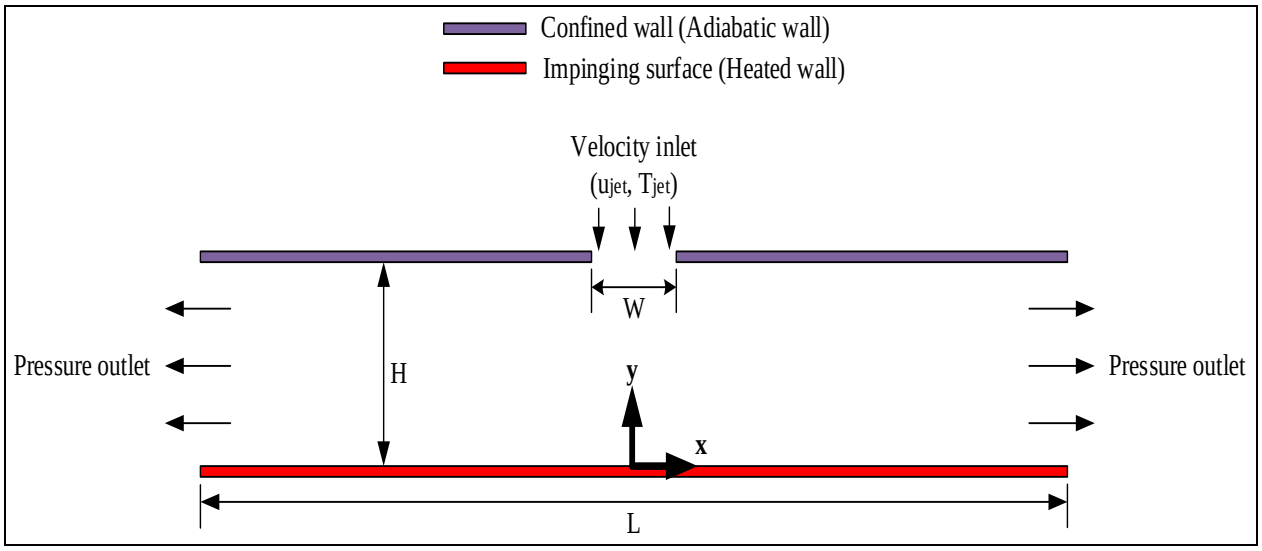

Figure 1. Schematic diagram of the physical model

2.2. Boundary Conditions

It is assumed that there is a constant temperature, T_{jet} =293 K, and velocity, u_{jet}, at the channel's entrance. At the end of the channel, the pressure outlet condition is taken into account. The temperature of the bottom wall, T_{imp} =343 K, is kept constant, and the no-slip condition is imposed. The top wall has an adiabatic condition and a non-slip surface.

2.3. Governing Equations

The current investigation takes into account flow circumstances that are described as single-phase, turbulent, incompressible, steady-state, and constant in their properties. The equations that determine continuity, momentum, and energy are solved using cartesian coordinates, which are as follows [14]:

Continuity:

$$\frac{\partial}{\partial x_i}(\rho u_i) = 0 \tag{1}$$

Momentum:

$$\frac{\partial}{\partial x_j}\left(\rho u_i u_j\right) = -\frac{\partial P}{x_i} + \frac{\partial}{\partial x_j}\left\{\mu\left(\frac{\partial u_i}{\partial x_j} + \frac{\partial u_j}{\partial x_i} - \frac{2}{3}\delta_{ij}\frac{\partial u_i}{\partial x_j}\right)\right\} + \frac{\partial}{\partial x_j}\left(-\rho\overline{u_i' u_j'}\right) \tag{2}$$

Energy:

$$\frac{\partial}{\partial x_i}\{u_i(\rho E + P)\} = \frac{\partial}{\partial x_j}\left\{\left(\lambda + \frac{C_p \mu_t}{Pr_t}\right)\right\}\frac{\partial T}{\partial x_j} + u_i(\tau_{ij})_{eff} \tag{3}$$

where $(\tau_{ij})_{eff}$ and E are the deviatoric stress tensor and total energy, respectively, and their formula is given below:

$$(\tau_{ij})_{eff} = \mu_{eff}\left(\frac{\partial u_j}{\partial x_i} + \frac{\partial u_i}{\partial x_j}\right) - \frac{2}{3}\mu_{eff}\frac{\partial u_i}{\partial x_j}\delta_{ij} \tag{4}$$

$$E = C_p T - \frac{P}{\rho} + \frac{u^2}{2} \tag{5}$$

The $k - \varepsilon$ standard turbulence model is used in this study. Below are the equations for transport for the turbulence model [15]:

$$\frac{\partial}{\partial t}(\rho k) + \frac{\partial}{\partial x_i}(\rho k u_i) = \left\{\frac{\partial}{\partial x_j}\left(\mu + \frac{\mu_t}{\sigma_k}\right)\frac{\partial k}{\partial x_i}\right\} + (G_k + G_b) - \rho\varepsilon - Y_m + S_\varepsilon \tag{6}$$

$$\frac{\partial}{\partial t}(\rho\varepsilon)+\frac{\partial}{\partial x_i}(\rho\varepsilon u_i)=\left\{\frac{\partial}{\partial x_j}\left(\mu+\frac{\mu_t}{\sigma_\varepsilon}\right)\frac{\partial\varepsilon}{\partial x_i}\right\}+C_{1\varepsilon}\frac{\varepsilon}{k}(G_k+C_{3\varepsilon}G_b)-C_{2\varepsilon}\rho\frac{\varepsilon^2}{k}+S_\varepsilon \quad (7)$$

where G_b is the energy produced by buoyancy, G_k is the energy produced by mean-velocity gradients, and Y_m is the rate of change associated with the total turbulent thermal energy lost. σ_k=1.0 and σ_ε=1.3 are the turbulent Prandtl numbers for k and ε, respectively. $C_{1\varepsilon}$=1.44 and $C_{2\varepsilon}$ =1.92 are constants. $C_{3\varepsilon}$ represents the dependence rate of ε on buoyancy, and it is determined from the following equation:

$$C_{3\varepsilon}=tanh\left|\frac{v}{u}\right| \quad (8)$$

The turbulent viscosity is obtained from the following equation:

$$\mu_t=\rho C_\mu\frac{k^2}{\varepsilon} \quad (9)$$

where C_μ=0.09 is the constant parameter.

3. DETERMINATION OF THERMOPHYSICAL PROPERTIES OF THE NANOFLUID

Water or a solution containing $CoFe_3O_2$ nanoparticles with 2% and 4% *napv* serves as the working fluid. Table 1 reports water and $CoFe_3O_2$'s density, specific heat, dynamic viscosity, and thermal conductivity. When nanoparticles are present, the characteristics of the working fluid may change depending on the concentration of the particles. Since nanofluids may be treated as Newtonian fluids for low-volume fractions (up to 10%) and minor temperature changes. A single-phase model is used. As a result, in order to calculate the thermal and physical characteristics of the nanofluids under consideration, it is required to apply relations accessible in the literature as given below.

Table 1. Thermophysical properties of water and $CoFe_3O_2$ nanoparticle

Properties	ρ (kg/m^3)	k (W/mK)	C_p (J/kgK)	$Pr=(C_p\mu)/k$
Water [16]	997.1	0.6071	4180	6.8
$CoFe_3O_2$ [17]	4907	3.7	700	-

3.1. Density

The nanofluid density is determined from the following equation [18]:

$$\rho_{nf} = (1-\varphi)\rho_f + \varphi\rho_p \tag{10}$$

where ρ and φ are density and *napv*, respectively. The subscripts of *nf*, *f*, and *p* denote nanofluid, water, and nanoparticle, respectively.

3.2. Specific Heat

Specific heat of the nanofluid may be obtained from Eq. (11) [18].

$$C_{p_{nf}} = \frac{(1-\varphi)\rho_f C_{p_f} + \varphi\rho_p C_{p_p}}{\rho_{nf}} \tag{11}$$

where C_p represents specific heat.

3.3. Thermal Conductivity

The thermal conductivity lamina shaped $CoFe_3O_2$/water nanofluid is determined from the following formula [19]:

$$\frac{k_{nf}}{k_f} = \frac{[k_p+(m-1)]-(m-1)\varphi(k_f-k_p)}{[k_p+(m-1)k_f]+\varphi(k_f-k_p)} \tag{12}$$

where m is the shape factor. m=16.1576 [19] for the lamina-shaped nanoparticles.

3.4. Viscosity

The viscosity of the $CoFe_3O_2$/water nanofluid is obtained from the equation given below [18] and μ_f is determined from Prandtl number equation given in Table 1.

$$\mu_{nf} = \frac{\mu_f}{(1-\varphi)^{2.5}} \tag{13}$$

4. NUMERICAL PROCEDURE

4.1. Numerical Algoritm

The fundamental differential equations of the issue under investigation are the continuity, momentum, energy, and turbulence equations; they are solved numerically in this investigation by using the boundary conditions of the problem. Computational fluid dynamics (CFD) software from the Fluent package is utilized for this objective. Numerical modeling employs several turbulence models, among which the $k-\varepsilon$ turbulence model is extensively utilized due to its cost-effectiveness and ability to produce reasonably accurate results in numerous flow scenarios [20]. Thus, the $k-\varepsilon$ standard turbulence model is utilized as the basis for the model of turbulence. For the equations of energy and momentum, the second-order upwind method is utilized. It has been decided to connect pressure and velocity using the SIMPLE algorithm. For the convergence of numerical solutions, the convergence criterion is 10^{-6}.

4.2. Grid Independence Test and Validation

As a means of determining whether or not the grid number has any effect on the numerical analysis outcomes, many grid numbers with varying numbers of elements are built at *Re*=24000 for water. Table 2 displays the combined findings for all of these grid number. After the research, G4 is selected as the optimal grid. The $y^+<1$ criterion is met by the first layer close to the wall. Any analyses performed within the scope of this investigation will now be allowed to utilize this optimal grid number.

Table 2. Test of grid independence

Grid name	Grid number	*Nu*	*Nu* Deviation (%)	*Dff*	*Dff* Deviation (%)
G1	5268	55.369	-	0.016258	-
G2	25423	72.258	23.373	0.012589	-29.144
G3	62482	81.269	11.087	0.011267	-11.733
G4	110065	82.462	1.446	0.011122	-1.303
G5	230124	83.256	0.953	0.011136	0.125
G6	578359	83.126	-0.00156	0.01123	0.837

Validation is accomplished by comparing the current findings to numerical studies by Manca et al. [21] under identical conditions (*Re*=5000–20000 and H/W = 4). Figure 2 shows the comparisons that are made. Figure 2 demonstrates that the present findings agree well with the

literature. Based on these comparative findings, it can result that the model suggested in the current investigation is credible, and it will be used as the basis for future numerical assessments.

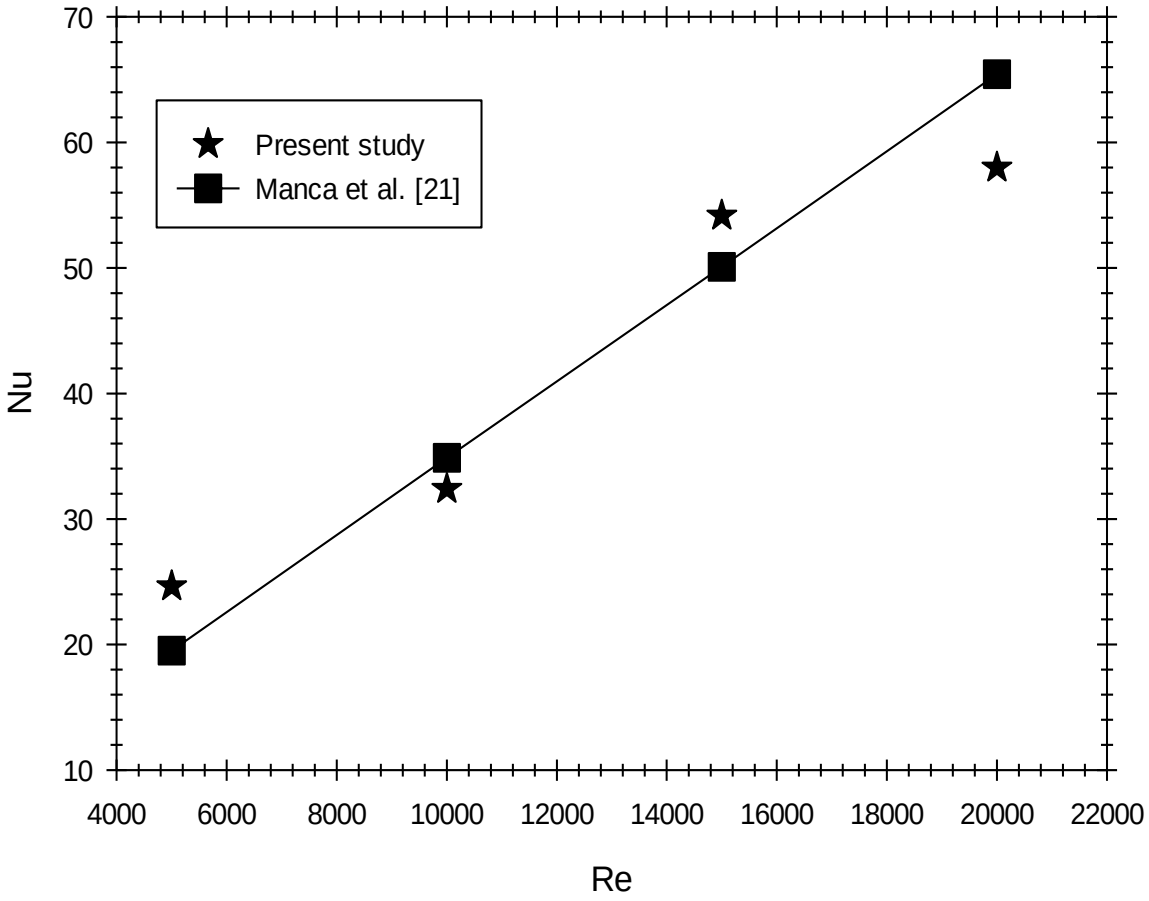

Figure 2. Validation of the study

4.3. Data Reduction

The *Re* is determined from the following equation:

$$Re = \frac{\rho u_{jet} W}{\mu} \tag{14}$$

where W and u_{jet} represent the jet inlet width and velocity, respectively.

The *Nu* equation can be written as below:

$$Nu = \frac{q'' W}{k(T_{imp} - T_{jet})} \tag{15}$$

where T_{imp} and T_{jet} denote the temperature of impinging surface and jet, respectively. q'' is the heat flux of the impinging surface.

Darcy friction factor (*Dff*) equation can be stated as below:

$$Dff = \frac{2(\Delta P)W}{\rho L u_{jet}^2} \tag{16}$$

where ΔP and L are the pressure difference and length of the impinging surface, respectively.

5. RESULTS AND DISCUSSION

Following are presentations and discussions of the flow and heat transfer fields with varying *Re*s (6000–24000), working fluids (water and $CoFe_3O_2$/water nanofluid), and *napv*s (φ= 2-4%). Also, temperature contours, velocity streamlines, and entropy generation contours are given and discussed in detail.

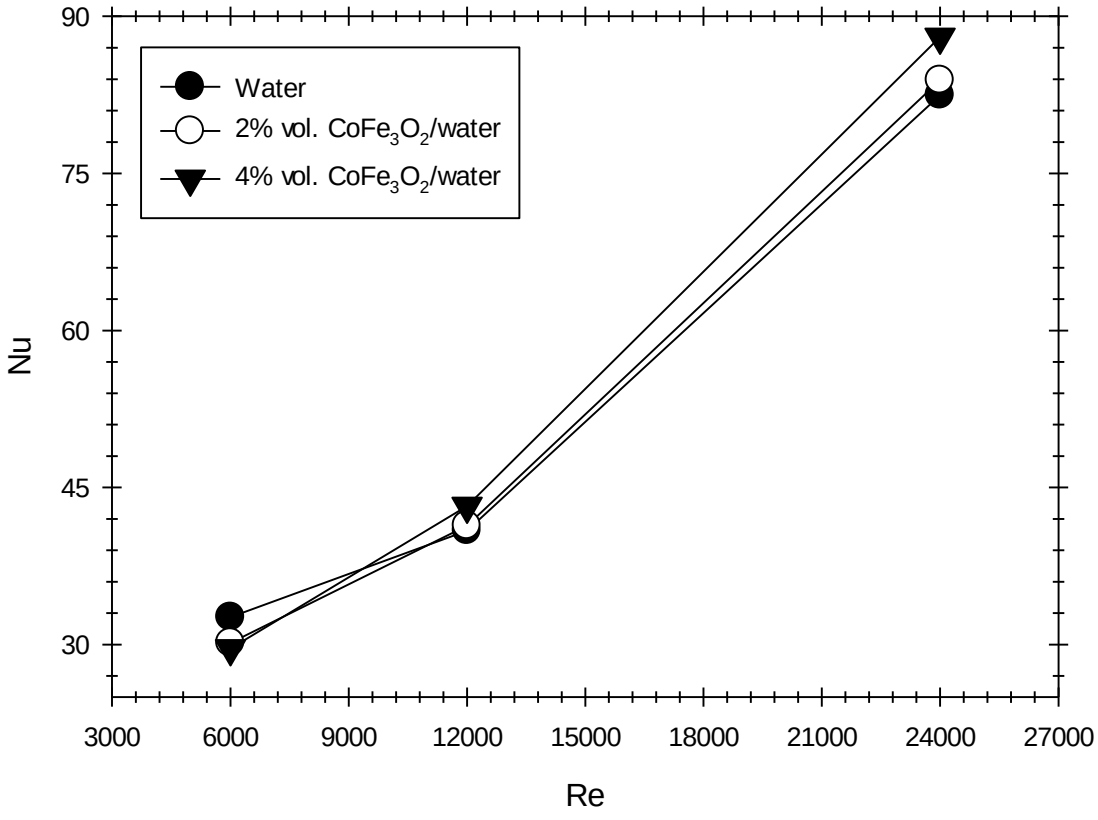

Figure 3. Influence of the different working fluids and their *napv*s on *Nu*

In Figure 3, the varying distribution of *Nu* depending on different *Re*s and different working fluids is given. Looking at the graph, the *Nu* increases for water and $CoFe_3O_2$/water nanofluid. As the *Re* increases, the fluid velocity increases. Turbulence increases due to the increase in fluid velocity. As a result, convective heat transfer increases. However, a larger increase in the *Re* caused a further increase in the *Nu* [22]. For example, when the *Nu* for water is compared with the values of *Re*=6000 and *Re*=12000, the *Nu* increases by 20.18%. Likewise, when *Re*=12000 and *Re*=24000 are compared, the *Nu* shows an increase of 50.43%. It has been determined that the use of different working fluids affects the *Nu*. In addition, it can be seen that 2.0% and 4.0% *napv* also have an effect. Using $CoFe_3O_2$/water nanofluid as the working fluid shows an increase over the *Nu* for all other *Re*s except *for Re*=6000. The reason why the *Nu* at *Re*=6000 is lower for $CoFe_3O_2$/water than for water is explained by looking at Eq. (15). The heat transfer coefficient at *Re*=6000 consists of a percentage increase less than that of the thermal conductivity coefficient. In other *Re*s (12000 and 24000), the *Nu* of $CoFe_3O_2$/water is higher than that of water, since the heat transfer coefficient shows a higher percentage increase than the thermal conductivity coefficient. At the highest *Re*, the *Nu* is 1.71% and 6.33% higher when using $CoFe_3O_2$/water with a *napv* of 2.0% and 4.0% compared to water. Such an increase in *Nu* is obtained because the thermal conductivity coefficient of the working fluid increased with the addition of nanoparticles to the water.

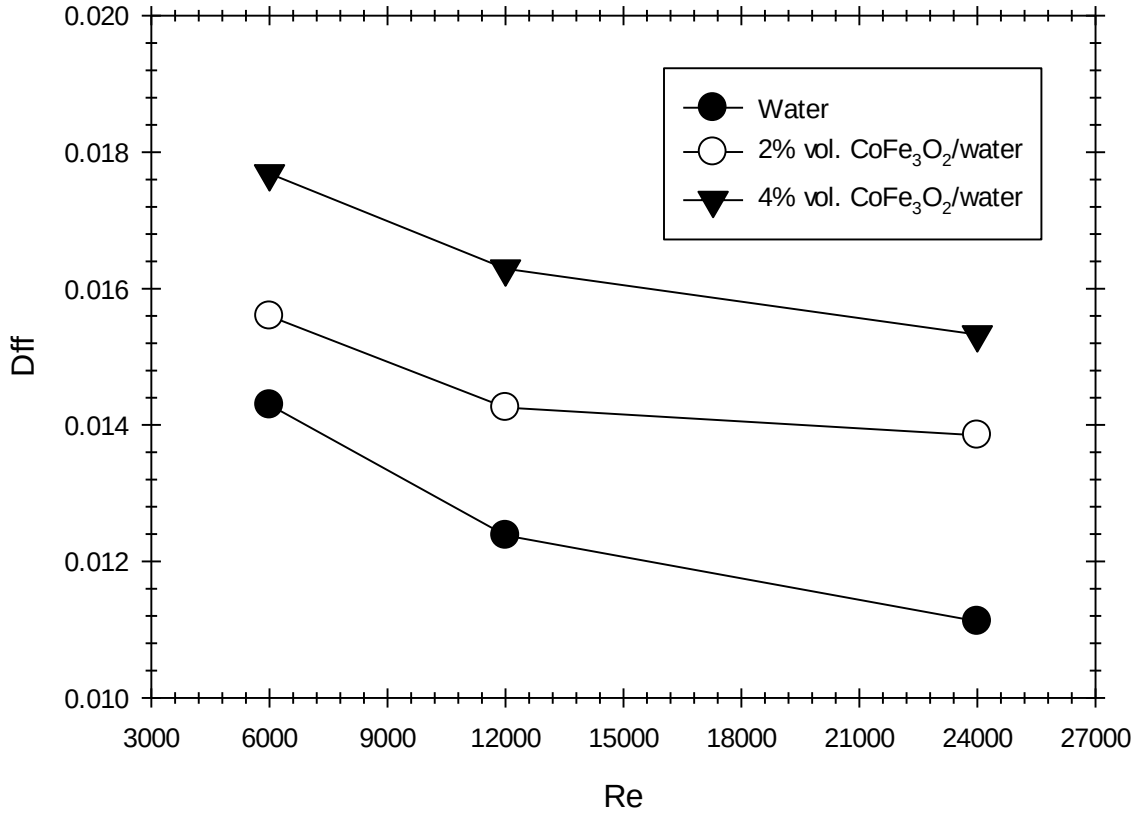

Figure 4. Effect of the different working fluids and their *napv*s on *Dff*

The variation of *Dff* as a function of *Re* in the different working fluids and *napv* is given in Figure 4. Looking at the graph, the *Dff* value decreases with increasing *Re* for water and $CoFe_3O_2$/water nanofluid. When $CoFe_3O_2$/water nanofluid is used, the *Dff* value increases compared to water. The reason for this can be interpreted as the higher viscosity value of the newly formed working fluid when $CoFe_3O_2$ nanoparticles are added to the water. Based on comparisons with water data, the *Dff* increase at 2.0% concentrations is 8.33% (*Re*=6000), 13.28% (*Re*=12000), and 19.56% (*Re*=24000). The *Dff* increases by 19.21% (*Re*=6000), 23.92% (*Re*=12000), and 27.45% (*Re*=24000) compared to water data at 4.0% concentration.

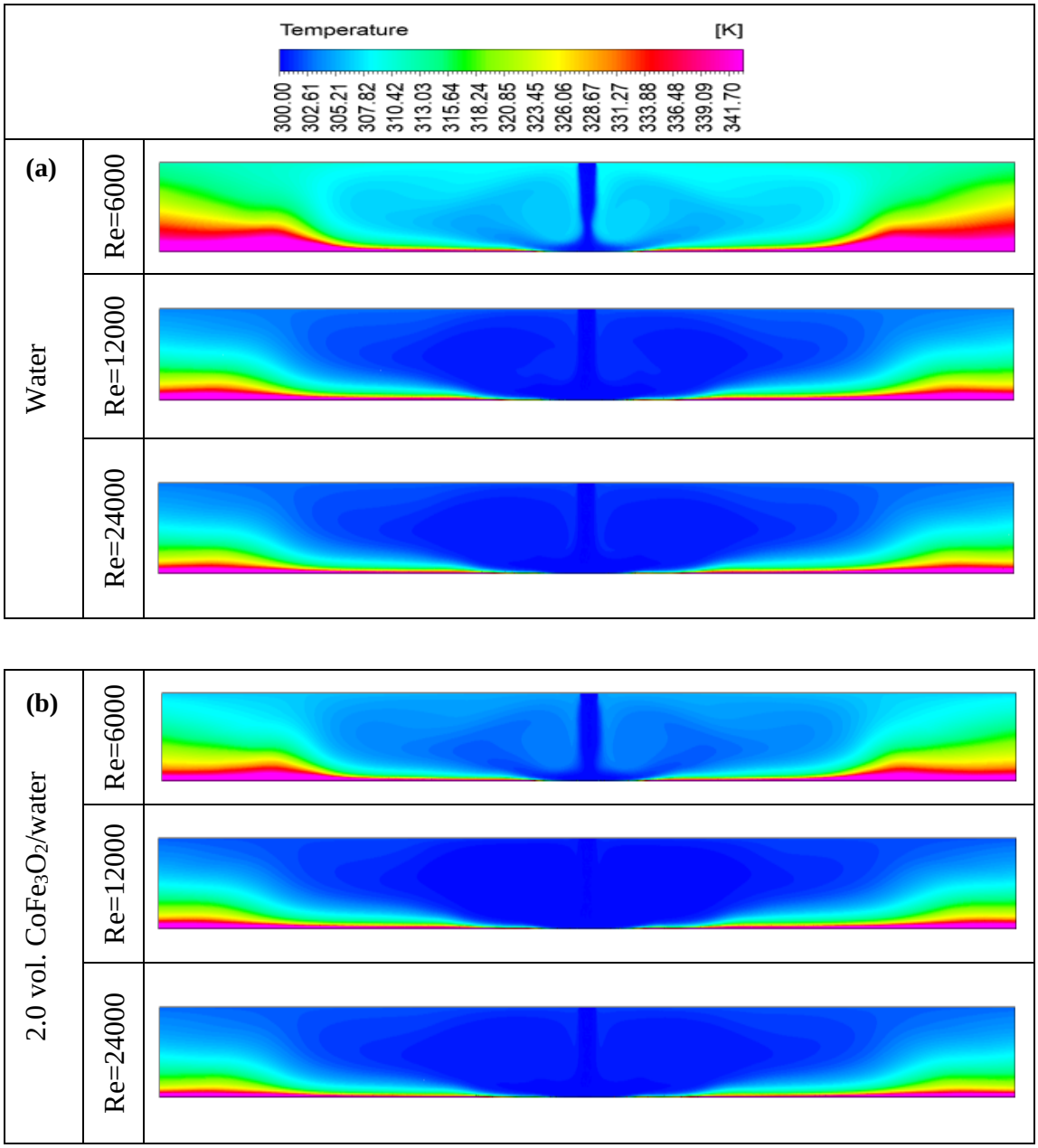
Temperature
[K]
300.00
302.61
305.21
307.82
310.42
313.03
315.64
318.24
320.85
323.45
326.06
328.67
331.27
333.88
336.48
339.09
341.70
(a)
Water
Re=6000
Re=12000
Re=24000
(b)
2.0 vol. CoFe3O2/water
Re=6000
Re=12000
Re=24000

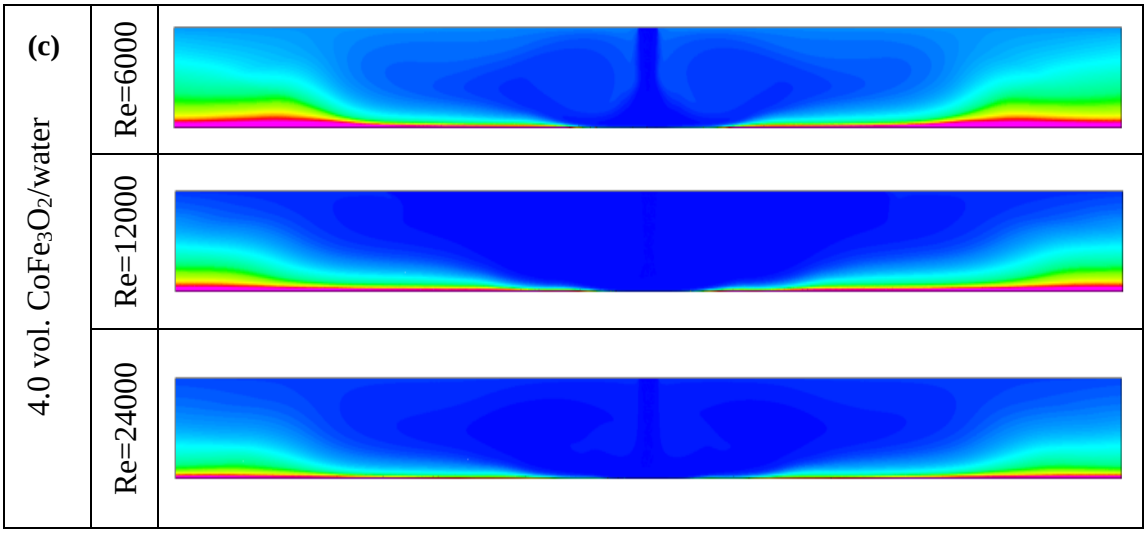

Figure 5. Temperature contour of (a) water, (b) 2.0% vol. $CoFe_3O_2$/water, and (c) 4.0% vol. $CoFe_3O_2$/water for different *Re*s

Figures 5(a)-(c) exhibit the temperature contours at different *Re*s for the study with water, 2.0% vol. $CoFe_3O_2$/water, and 4.0% vol. $CoFe_3O_2$/water as the working fluids, respectively. As can be seen from the contours, the temperature on the impinging surface decreases more with the increase of *Re* in all working fluids. In other words, it can be said that the temperature distribution becomes more uniform. When $CoFe_3O_2$/water nanofluid is used instead of water, the fluid velocity increases depending on the thermophysical properties of the nanofluid. This velocity increase further reduces the temperature on the impinging surface compared to water. The increase in *napv* from 2.0% to 4.0% also made the temperature distribution in the system uniform. In addition, the thermal boundary layer thickness decreases by using nanofluids with different *napv* instead of water. As a result, the heat transfer between the impinging surface and the working fluid increases.

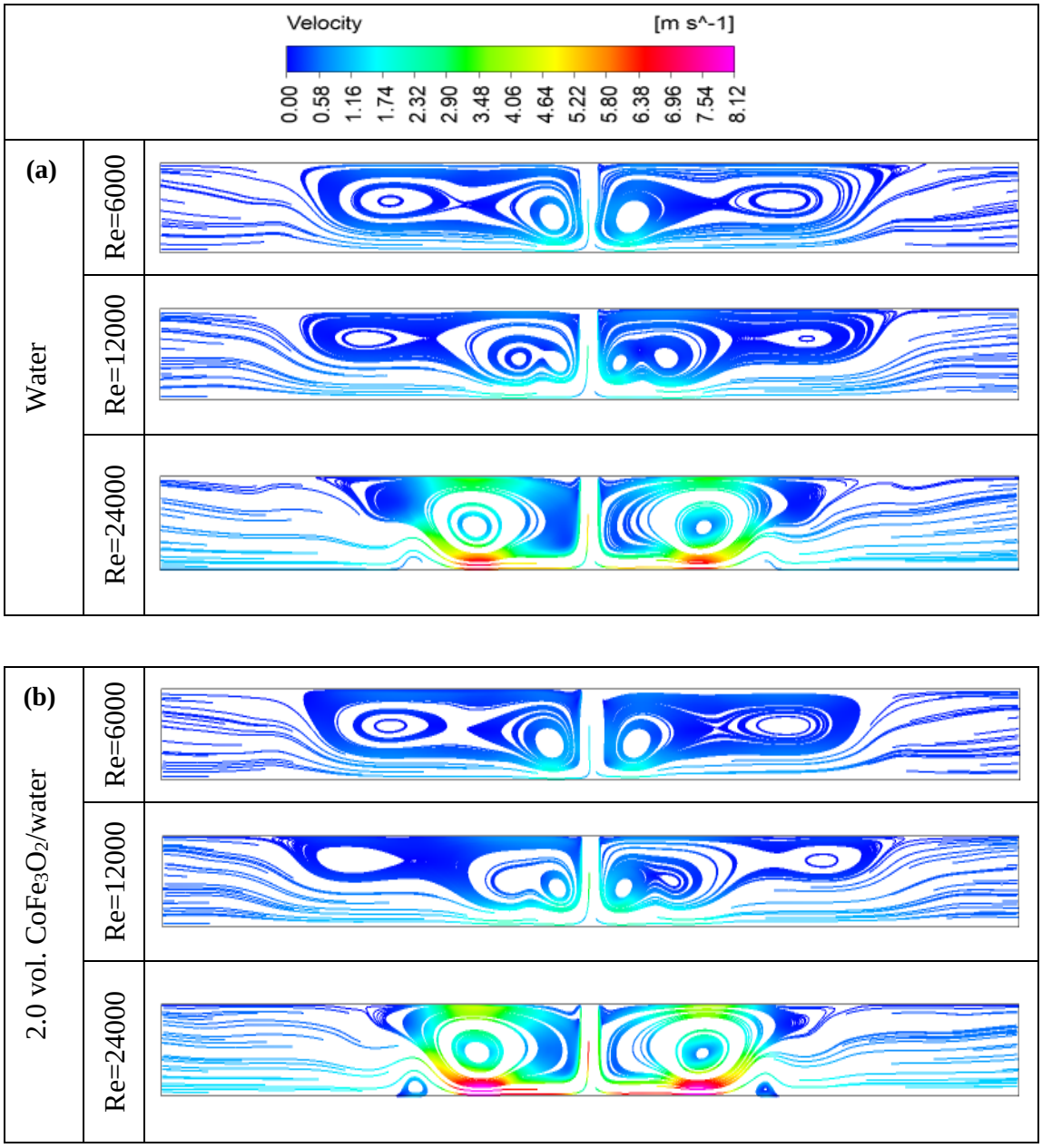
Velocity
[m s^-1]
0.00
0.58
1.16
1.74
2.32
2.90
3.48
4.06
4.64
5.22
5.80
6.38
6.96
7.54
8.12
(a)
Water
Re=6000
Re=12000
Re=24000
(b)
2.0 vol. CoFe3O2/water
Re=6000
Re=12000
Re=24000

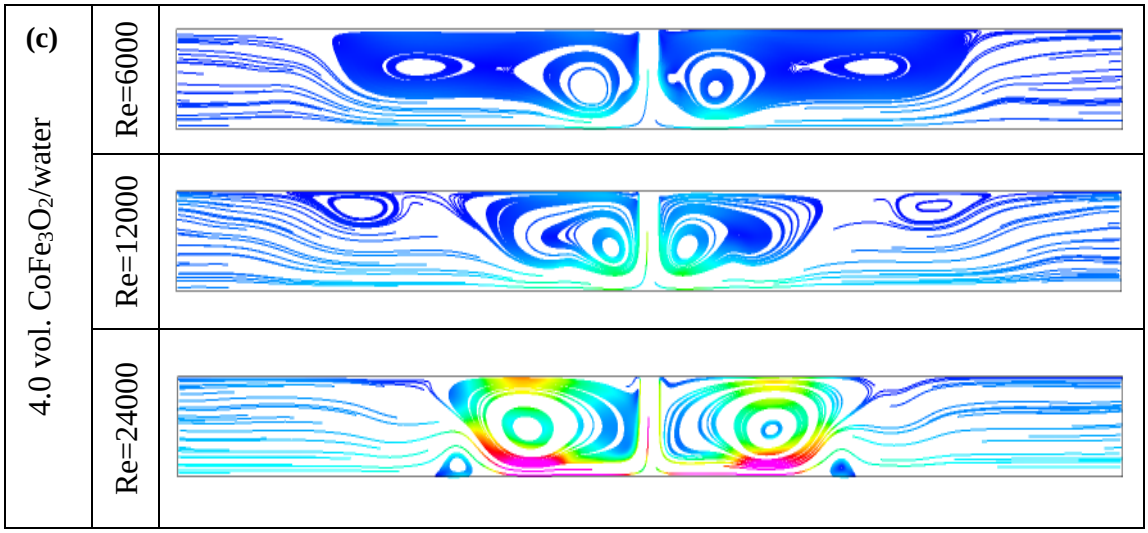

Figure 6. Velocity streamlines of (a) water, (b) 2.0% vol. $CoFe_3O_2$/water, and (c) 4.0% vol. $CoFe_3O_2$/water for different *Re*s

Figures 6(a)-(c) represent the velocity streamlines at different *Re*s for the study with water, 2.0% vol. $CoFe_3O_2$/water, and 4.0% vol. $CoFe_3O_2$/water as the working fluids, respectively. In all working fluids, the velocity increases with increasing *Re*. Especially 2.0% vol. $CoFe_3O_2$/water and 4.0% vol. $CoFe_3O_2$/water, it is seen that the velocity of $CoFe_3O_2$/water nanofluids is higher than that of water. As a result, the *Nu*, or convective heat transfer, is higher in nanofluids than in water. In addition, it can be determined that the *napv* increases from 2.0% to 4.0%, which increases the fluid velocity. When $CoFe_3O_2$/water is used and Re=6000 and Re=12000, two recirculation zones are formed. With the increase of the *Re*, the center of one of these recirculation zones (on the left) shifts upward (towards the adiabatic wall), while the center of the other recirculation surface (impinging surface moves downwards.) slides. The approach of the recirculation zones towards the impinging surface increases the heat transfer that will occur on the impinging surface. In *Re*=24000 and all working fluids, a recirculation zone also occurred on the impinging surface.

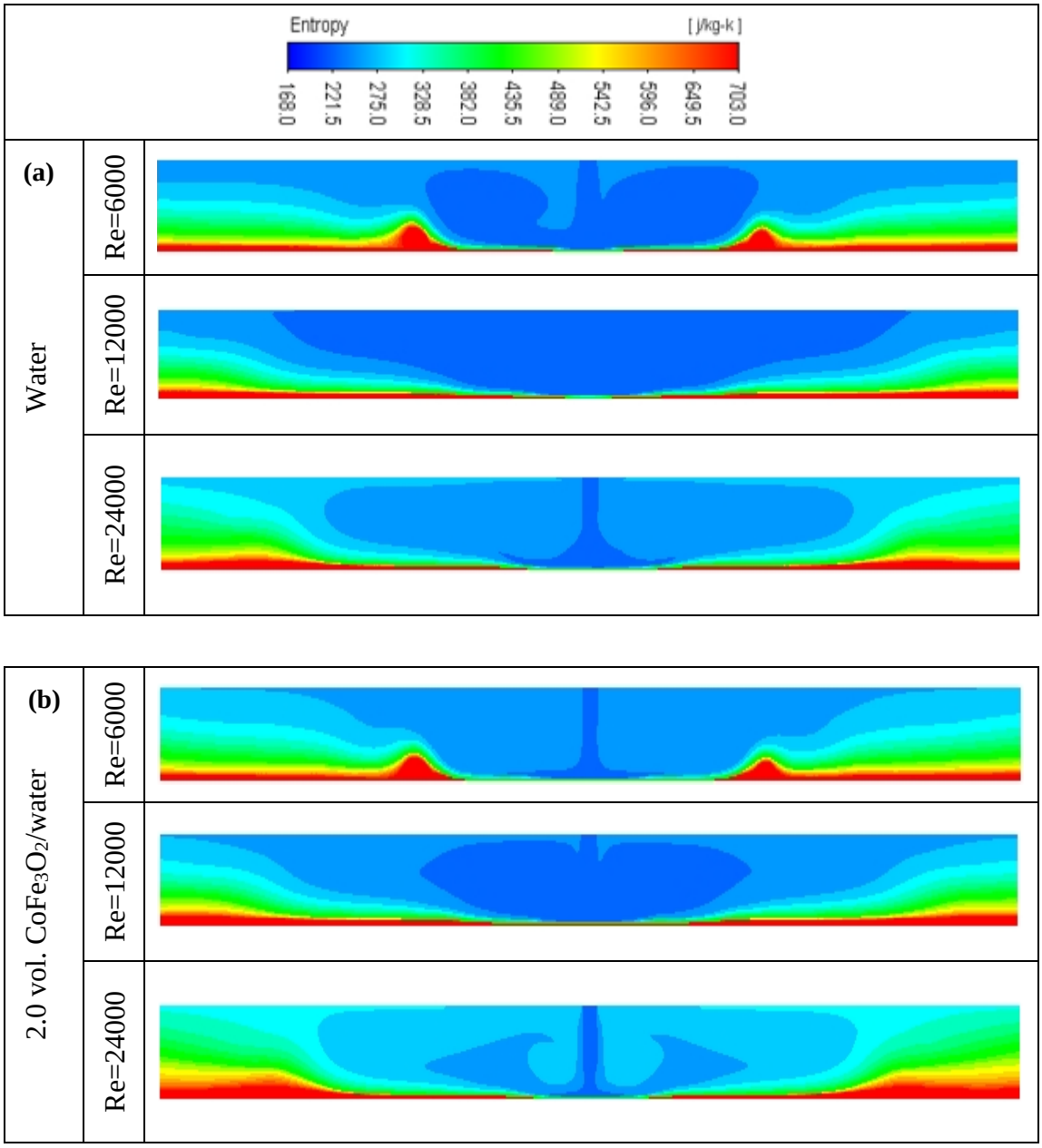
Entropy
[J/kg-k]
168.0
221.5
275.0
328.5
382.0
435.5
489.0
542.5
596.0
649.5
703.0
(a)
Water
Re=6000
Re=12000
Re=24000
(b)
2.0 vol. CoFe3O2/water
Re=6000
Re=12000
Re=24000

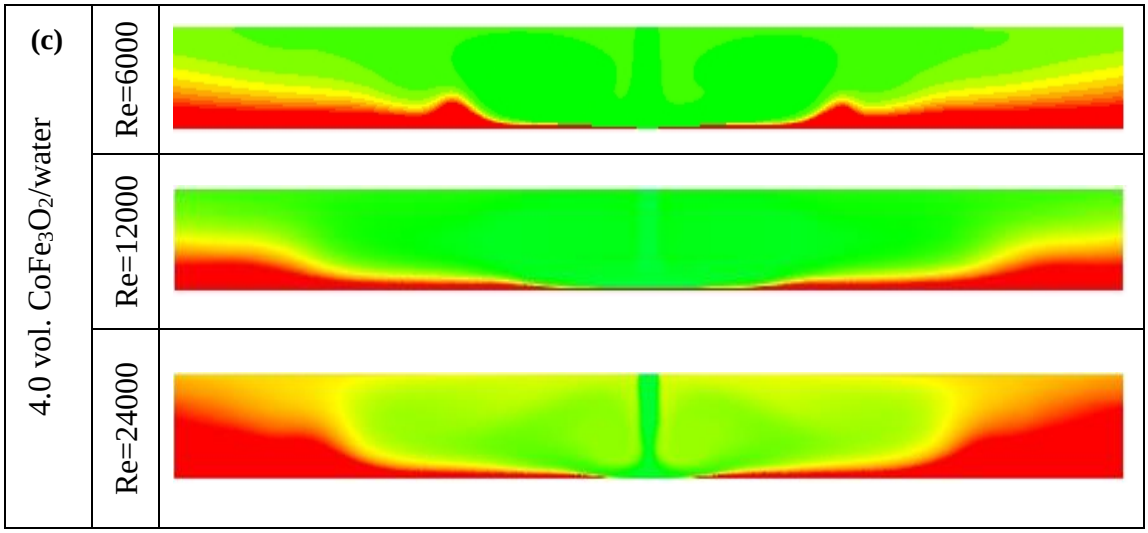

Figure 7. Entropy generation of (a) water, (b) 2.0% vol. $CoFe_3O_2$/water, and (c) 4.0% vol. $CoFe_3O_2$/water for different *Re*s

Figures 7(a)-(c) present the entropy generation contours at different *Re*s for the study with water, 2.0% vol. $CoFe_3O_2$/water, and 4.0% vol. $CoFe_3O_2$/water as the working fluid, respectively. Looking at the graph, the increase in entropy generation with the increase of the *Re* for all working fluids draws attention. This result shows that working at low *Re* is more advantageous in a way. With the use of $CoFe_3O_2$/water nanofluid, it can be easily seen that the red color contours increase and the blue color contours decrease. Since the irreversibilities of fluid friction and heat transfer increase with the increase in velocity and temperature gradients, respectively, the entropy production rises with *Re*. In addition, increasing the *napv* from 2.0% to 4.0% also grows entropy production. The results of the entropy generation are compatible with [23].

3. CONCLUSION

The *Nu*, *Dff*, temperature, entropy generation contours, and velocity streamline the distribution of impinging lamina-shaped nanofluid ($CoFe_3O_2$/water) and pure water jets are conducted in this study. Listed below are the most important outcomes of the present framework.

- As compared to water, utilizing $CoFe_3O_2$/water with a *napv* of 2.0% or 4.0% results in a *Nu* that is 1.71% and 6.33% greater, respectively, than when using water alone at the maximum *Re*.
- For both water and $CoFe_3O_2$/water nanofluid, the value of *Dff* drops as the *Re* rises. A higher *Dff* value is achieved when a $CoFe_3O_2$/water nanofluid is employed instead of pure water.

- In all working fluids, the increment in entropy production with increasing *Re* is due to the fluid friction and heat transfer enhancement.

NOMENCLATURE

W	Width of the jet inlet (m)
H	Height of the channel (m)
L	Length of the channel (m)
T	Temperature (K)
μ	Dynamic viscosity (Pa.s)
δ	Kronecher delta function
u	Velocity (m/s)
Re	Reynolds number
ρ	Density (kg/m^3)
C_p	Specific heat (J/kgK)
Pr	Prandtl number
k	Thermal conductivity coefficient (W/mK)
P	Pressure (Pa)
φ	Nanoparticle volume fraction
m	shape factor
Nu	Nusselt number
Dff	Darcy friction factor
q''	Heat flux (W/m^2)
x,y	Spatial coordinates (m)

Subscripts

imp	Impinging surface
nf	Nanofluid
f	Base fluid
p	Nanoparticle

Abbreviations

napv	Nanoparticle volume fraction

DECLARATION OF ETHICAL STANDARDS

The author of the paper submitted declares that nothing necessary for achieving the paper requires ethical committee and/or legal-special permissions.

CONTRIBUTION OF THE AUTHOR

Recep Ekiciler: Performed the computations, analyzed the results and wrote the manuscript.

CONFLICT OF INTEREST

There is no conflict of interest in this study.

REFERENCES

[1] El-Maghlany WM, Sorour MM, Abbass AM, Alnakeeb MA. Numerical study of free surface axisymmetric jet impinging on a heated flat surface utilizing high concentration SiO_2 nanofluid. Journal of the Taiwan Institute of Chemical Engineers 2022; 135: 104401.

[2] Zeitoun O, Ali M, Al-Ansary H. The effect of particle concentration on cooling of a circular horizontal surface using nanofluid jets. Nanoscale and Microscale Thermophysical Engineering 2013; 17: 154–171.

[3] Nguyen CT, Galanis N, Polidori G, Fohanno S, Popa CV, Le Bechec A. An experimental study of a confined and submerged impinging jet heat transfer using Al_2O_3-water nanofluid. International Journal of Thermal Sciences 2009; 48: 401–411.

[4] Selimefendigil F, Öztop HF. Jet impingement cooling and optimization study for a partly curved isothermal surface with CuO-water nanofluid. International Communications in Heat and Mass Transfer 2017; 89: 211–218.

[5] Tie P, Li Q, Xuan Y. Heat transfer performance of Cu–water nanofluids in the jet arrays impingement cooling system. International Journal of Thermal Sciences 2014; 77: 199–205.

[6] Khatak P, Jakhar R, Kumar M. Enhancement in cooling of electronic components by nanofluids. Journal of the Institution of Engineers (India): Series C 2015; 96: 245–251.

[7] Yousefi-Lafouraki B, Ramiar A, Mohsenian S. Entropy generation analysis of a confined slot impinging jet in a converging channel for a shear thinning nanofluid. Applied Thermal Engineering 2016; 105: 675–685.

[8] Gherasim I, Roy G, Nguyen CT, Vo-Ngoc D. Heat transfer enhancement and pumping power in confined radial flows using nanoparticle suspensions (nanofluids). International Journal of Thermal Sciences 2011; 50: 369–377.

[9] Faris M, Zulkifli R, Harun Z, Abdullah S, Aizon WG, Abbas AA. Experimental investigation on comparison of local nusselt number using twin jet impingement mechanism. International Journal of Mechanical & Mechatronics Engineering IJMME-IJENS 2017; 17: 60–75.

[10] Singh MK, Yadav D, Arpit S, Mitra S, Saha SK. Effect of nanofluid concentration and composition on laminar jet impinged cooling of heated steel plate. Applied Thermal Engineering 2016; 100: 237–246.

[11] Rehman MMU, Qu ZG, Fu RP, Xu HT. Numerical study on free-surface jet impingement cooling with nanoencapsulated phase-change material slurry and nanofluid. International Journal of Heat and Mass Transfer 2017; 109: 312–325.
[12] Akinshilo A. Geometry shape effects of nanoparticles on fluid heat transfer through porous channel. AUT Journal of Mechanical Engineering 2020; 4(1): 41-50.
[13] Rashid U, Lu D, Iqbal Q. Nanoparticles impacts on natural convection nanofluid flow and heat transfer inside a square cavity with fixed a circular obstacle. Case Studies in Thermal Engineering 2023; 44: 102829.
[14] ANSYS Fluent Theory Guide. Lebanon, New Hampshire: Fluent Corporation; 2006.
[15] Launder BE, Spalding DB. Paper 8 - The numerical computation of turbulent flows. In: Patankar SV, Pollard A, Singhal AK, Vanka SP, editors. Numerical Prediction of Flow, Heat Transfer, Turbulence and Combustion, Pergamon 1983; 96–116.
[16] Yusuf TA, Mabood F, Khan WA, Gbadeyan JA. Irreversibility analysis of Cu-TiO_2-H_2O hybrid-nanofluid impinging on a 3-D stretching sheet in a porous medium with nonlinear radiation: Darcy-Forchhiemer's model. Alexandria Engineering Journal 2020; 59: 5247–5261.
[17] Waqas H, Farooq U, Naseem R, Hussain S, Alghamdi M. Impact of MHD radiative flow of hybrid nanofluid over a rotating disk. Case Studies in Thermal Engineering 2021; 26: 101015.
[18] Tan Z, Jin P, Zhang Y, Xie G. Flow and thermal performance of a multi-jet twisted square microchannel heat sink using CuO-water nanofluid. Applied Thermal Engineering 2023; 225: 120133.
[19] Rashid U, Liang H, Ahmad H, Abbas M, Iqbal A, Hamed YS. Study of (Ag and TiO_2)/water nanoparticles shape effect on heat transfer and hybrid nanofluid flow toward stretching shrinking horizontal cylinder. Results In Physics 2021; 21: 103812.
[20] Karabulut K. Heat transfer increment study taking into consideration fin lengths for CuO-water nanofluid in cross flow-impinging jet flow channels. Thermal Science 2023: 35–35.
[21] Manca O, Mesolella P, Nardini S, Ricci D. Numerical study of a confined slot impinging jet with nanofluids. Nanoscale Research Letters 2011; 6: 188.
[22] Kareem ZS, Balla HH, AbdulWahid AF. Heat transfer enhancement in single circular impingement jet by CuO-water nanofluid. Case Studies in Thermal Engineering 2019; 15: 100508.
[23] Alabdaly IK, Ahmed MA. Numerical investigation on the heat transfer enhancement using a confined slot impinging jet with nanofluid. Propulsion and Power Research 2019; 8: 351–361.